Haverford College

Haverford Scholarship

2014

2MTF-IV. A Bulk Flow Measurement of the Local Universe

Karen Masters
Haverford College, klmasters@haverford.edu

Tao Hong

Christopher M. Springob

Repository Citation

2MTF – IV. A bulk flow measurement of the local Universe

Tao Hong,[1,2,3]★ Christopher M. Springob,[2,3,4] Lister Staveley-Smith,[2,3]
Morag I. Scrimgeour,[2,3,5,6] Karen L. Masters,[7,8] Lucas M. Macri,[9]
Bärbel S. Koribalski,[10] D. Heath Jones[11] and Tom H. Jarrett[12]

[1]*National Astronomical Observatories, Chinese Academy of Sciences, 20A Datun Road, Chaoyang District, Beijing 100012, China*

[2]*International Centre for Radio Astronomy Research, M468, University of Western Australia, Crawley, 35 Stirling Highway, WA 6009, Australia*

[3]*ARC Centre of Excellence for All-sky Astrophysics (CAASTRO), 44 Rosehill Street, Redfern, NSW 2016, Australia*

[4]*Australian Astronomical Observatory, PO Box 915, North Ryde, NSW 1670, Australia*

[5]*Department of Physics and Astronomy, University of Waterloo, Waterloo, ON N2L 3G1, Canada*

[6]*Perimeter Institute for Theoretical Physics, 31 Caroline St. N., Waterloo, ON N2L 2Y5, Canada*

[7]*Institute for Cosmology and Gravitation, University of Portsmouth, Dennis Sciama Building, Burnaby Road, Portsmouth PO1 3FX, UK*

[8]*South East Physics Network (www.sepnet.ac.uk), University of Portsmouth, Dennis Sciama Building, Burnaby Road, Portsmouth, PO1 3FX, UK*

[9]*George P. and Cynthia Woods Mitchell Institute for Fundamental Physics and Astronomy, Department of Physics and Astronomy, Texas A&M University, 4242 TAMU, College Station, TX 77843, USA*

[10]*CSIRO Astronomy & Space Science, Australia Telescope National Facility, PO Box 76, Epping, NSW 1710, Australia*

[11]*School of Physics, Monash University, Clayton, VIC 3800, Australia*

[12]*Astronomy Department, University of Cape Town, Private Bag X3. Rondebosch 7701, Republic of South Africa*

ABSTRACT

Using the 2MASS near-infrared photometry and high-signal-to-noise H I 21-cm data from the Arecibo, Green Bank, Nancay, and Parkes telescopes, we calculate the redshift-independent distances and peculiar velocities of 2018 bright inclined spiral galaxies over the whole sky. This project is part of the 2MASS Tully-Fisher survey (2MTF), aiming to map the galaxy peculiar velocity field within 100 h^{-1} Mpc, with an all-sky coverage apart from Galactic latitudes $|b| < 5°$. A χ^2 minimization method was adopted to analyse the Tully–Fisher peculiar velocity field in *J*, *H*, and *K* bands, using a Gaussian filter. We combine information from the three wavebands, to provide bulk flow measurements of 310.9 ± 33.9 , 280.8 ± 25.0, and 292.3 ± 27.8 km s^{-1} at depths of 20, 30, and 40 h^{-1} Mpc, respectively. Each of these bulk flow vectors points in a direction similar to those found by previous measurements. At each of the three depths, the bulk flow magnitude is consistent with predictions made by the Λ cold dark matter (ΛCDM) model at the 1σ level. The maximum likelihood and minimum variance method were also used to analyse the 2MTF samples, giving similar results.

Key words: surveys – galaxies: distances and redshifts – galaxies: spiral.

1 INTRODUCTION

Galaxy redshifts exhibit deviations from Hubble's law known as 'peculiar velocities', which are induced by the gravitational attraction of all surrounding matter. Peculiar velocities thus provide a means to trace the overall matter density field and detect all gravitating matter (both visible and dark). Peculiar velocities can be measured using redshift-independent distance indicators. Several such indicators have been used, including Type Ia SNe (Phillips 1993), the Tully–Fisher relation (TF; Tully & Fisher 1977) and the Fundamental Plane relation (FP; Djorgovski & Davis 1987; Dressler et al. 1987). The largest peculiar velocity surveys make use of ei-

ther the FP or TF relations. One limitation of these, and many other, redshift-independent distance indicators, however, is that they rely on optical photometry or spectroscopy. This means that the optical extinction effects of our Galaxy limit the sky coverage of such surveys in the so-called Zone of Avoidance (ZoA).

The 2MASS Tully-Fisher Survey (2MTF; Masters, Springob & Huchra 2008; Hong et al. 2013; Masters et al. 2014) is an all-sky TF survey aiming to measure the redshift-independent distances of nearby bright spiral galaxies. All galaxies in the 2MTF sample were selected from the 2MASS Redshift Survey (2MRS; Huchra et al. 2012), which is an extended redshift survey based on the 2 Micron All-Sky Survey Extended Source Catalog (Jarrett et al. 2000). By using the near-infrared (NIR) photometric data and high-quality 21-cm H I data from the Green Bank Telescope (GBT), Parkes radio telescope, Arecibo telescope, and other archival H I

catalogues, 2MTF provides sky coverage down to Galactic latitude $|b| = 5°$, which significantly reduces the area of the ZoA relative to previous TF surveys.

One parameter of the peculiar velocity field that benefits from the improved sky coverage of 2MTF is the dipole, or 'bulk flow'. In past measurements of the bulk flow of the local Universe, authors have largely agreed on the direction of the flow, but disagree on its amplitude (Hudson et al. 2004; Feldman, Watkins & Hudson 2010; Dai, Kinney & Stojkovic 2011; Ma, Branchini & Scott 2012; Ma & Scott 2013; Rathaus, Kovetz & Itzhaki 2013; Ma & Pan 2014). Watkins, Feldman & Hudson (2009) analysed a peculiar velocity sample of 4481 galaxies with a 'Minimum Variance' (MV) method, within a Gaussian window of radius 50 h^{-1} Mpc. They found a bulk flow with amplitude 407 ± 81 km s^{-1}, which they claim is inconsistent with the Λ cold dark matter (ΛCDM) model at >98 per cent confidence level.

On the other hand, other studies have shown a bulk flow amplitude agreeing with the ΛCDM model. By estimating the bulk flow of the SFI++ TF sample (Masters et al. 2006; Springob et al. 2007), Nusser & Davis (2011) derived a bulk flow of 333 ± 38 km s^{-1} at a depth of 40 h^{-1} Mpc, which is consistent with the ΛCDM model. Turnbull et al. (2012) adopted the bulk flow estimation on a Type Ia SNe sample with 245 peculiar velocity measurements, finding a bulk flow of 249 ± 76 km s^{-1}, which is also consistent with the expectation from ΛCDM.

In this paper, we use 2MTF data to measure the bulk flow in the local Universe. The relatively even sky coverage and uniform source selection criteria make 2MTF a good sample for bulk flow analysis. The data collection is described in Section 2. Section 3 introduces the calculations of TF distances and peculiar velocities. A χ^2 minimization method was adopted to analyse the peculiar velocity field, which is presented in Section 4. We compared our measurements with the ΛCDM predictions and previous measurements in Section 5. A summary is provided in Section 6.

Throughout this paper, we adopt a spatially flat cosmology with $\Omega_m = 0.27$, $\Omega_\Lambda = 0.73$, $n_s = 0.96$ (*WMAP*-7 yr; Larson et al. 2011). All distances in this paper are calculated and published in units of h^{-1} Mpc, where the Hubble constant is given by $H_0 = 100\,h$ km s^{-1} Mpc^{-1}. The observational results in this paper are independent of the actual value of h, though we compare with a ΛCDM model in Section 5 which assumes the *WMAP*-7 yr value of $h = 0.71$.

2 DATASETS

To build a high-quality peculiar velocity sample, all 2MTF target galaxies are selected from 2MRS using the following criteria: total K magnitudes $K < 11.25$ mag, $cz < 10\,000$ km s^{-1}, and axis ratio $b/a < 0.5$. There are $\sim$6000 galaxies that meet these criteria, but many of them are faint in H I, so observing the entire sample would be very expensive in terms of telescope time. We have combined archival H I data with observations from the Arecibo Legacy Fast ALFA survey (ALFALFA; Giovanelli et al. 2005) and new observations made with the GBT and Parkes radio telescope. The new observations preferentially targeted late-type spirals deemed likely to be H I rich, but the archival data includes all spiral subclasses. Accounting for galaxies eliminated from the sample because of confusion, marginal signal-to-noise ratio (SNR), non-detections, and other problematic cases, as well as cluster galaxies reserved for use in the 2MTF template (Masters et al. 2008), current peculiar velocity sample from 2MTF catalogue contains 2018 galaxies. As shown in Fig. 1, the catalogue provides uniform sky coverage down to Galactic latitude $|b| = 5°$, which makes it a good sample for bulk flow and large-scale structure analysis.

We note that the sample of 2018 galaxies discussed here is *separate* from the 888 cluster galaxies used to fit the template relation for 2MTF in Masters et al. (2008). The relationship between that template sample and the field sample is discussed further in Section 3.1.

2.1 Photometric data

All 2MTF photometric data are obtained from the 2MRS catalogue. 2MRS is an all-sky redshift survey based on 2MASS. It provides more than 43 000 redshifts of 2MASS galaxies, with $K < 11.75$ mag and $|b| \geq 5°$. The photometric quantities which are adopted for the TF calculations are the total magnitudes in J, H, and K bands, the 2MASS co-added axis ratio b/a (the axis ratio of $J+H+K$ image at the 3σ isophote; for more details see Jarrett et al. 2000) and the morphological type code T.
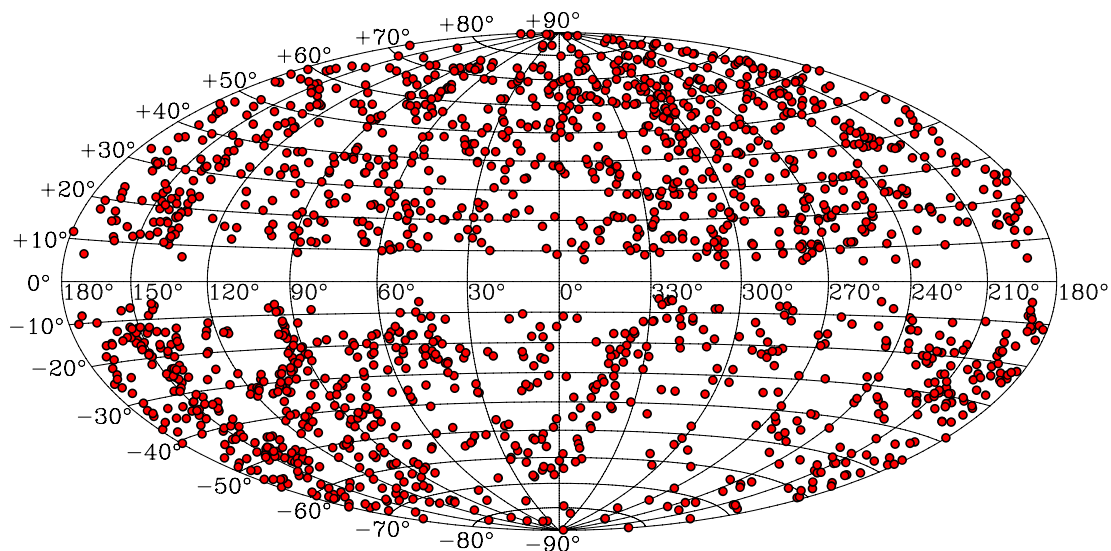
Figure 1. Sky coverage of the 2018 2MTF galaxies, in Galactic coordinates with an Aitoff projection.
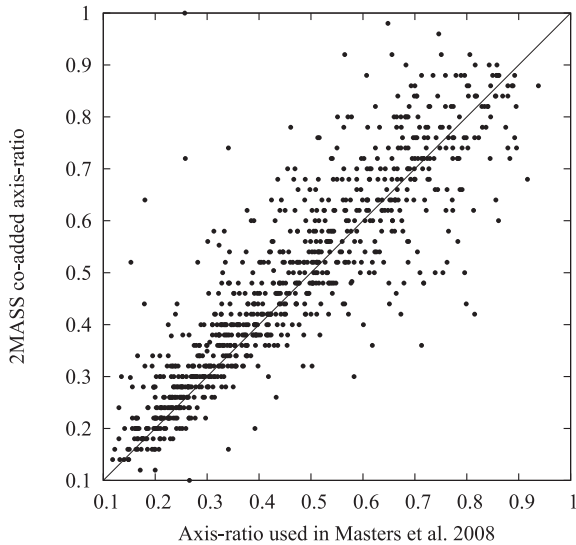
Figure 2. The comparison between the axis ratio adopted by Masters et al. (2008) and the 2MASS co-added axis ratio. The solid line indicates equality. 888 template galaxies used by Masters et al. (2008) are plotted here. The scatter of these two axis ratio is 0.096.

Masters et al. (2008) built the 2MTF TF template using the axis ratio in *I* band and *J* band. However, the *I*-band axis ratio are only available for a small fraction of the 2MTF non-template galaxies. Thus, to make the 2MTF non-template sample more uniform, we chose the 2MASS co-added axis ratio as our preferred data. As shown in Fig. 2, we took the 888 2MTF template galaxies as a comparison sample and compared the 2MASS co-added axis ratio with the axis ratio used in the 2MTF template. A dispersion was found between these two parameters ($\sim$0.096), which we expect will introduce a small scatter into the final TF relation, but no significant bias was detected in this comparison.

Galaxy internal dust extinction and *k*-correction were done following Masters et al. (2008). The total magnitudes provided by the 2MRS catalogue have already been corrected for Galactic extinction, so no additional such correction was applied here.

2.2 H I rotation widths

2.2.1 Archival data

Before making our new H I observations, we collected high-quality H I width measurements from the literature. The primary source of 2MTF archival data is the Cornell H I digital archive (Springob et al. 2005). The Cornell H I digital archive provides about 9000 H I measurements in the local Universe ($-200 < cz < 28\,000$ km s^{-1}) observed by single-dish radio telescopes. When cross-matching this H I data set with the 2MRS catalogue, we include only the galaxies with quality codes suggesting suitability of the measured width for TF studies, G (Good) and F (Fair) in the nomenclature of Springob et al. (2005). (See section 4 of that paper for details.) 1038 well-measured galaxies in this data set which meet the 2MTF selection criteria were taken into the final 2MTF catalogue. The H I widths provided by Springob et al. (2005) were corrected for redshift stretch, instrumental effects and smoothing, we have added the turbulence correction and viewing angle correction to make the corrected widths suitable for the TF calculations.

Besides the Cornell H I digital archive, we also collected H I data from Theureau et al. (1998, 2005, 2007), Mathewson, Ford

& Buchhorn (1992) and Nancay observed galaxies in table A.1 of Paturel et al. (2003). The raw observed widths taken from these sources were corrected for the aforementioned observational effects following Hong et al. (2013).

2.2.2 GBT and parkes observations

In addition to the archival H I data, new observations were conducted by the GBT and the Parkes radio telescope between 2006 and 2012.

1193 2MTF target galaxies in the region of $\delta > -40°$ were observed by the GBT (Masters et al. 2014) in position-switched mode, with the spectrometer set at nine level sampling with 8192 channels. After smoothing, the final velocity resolution was 5.15 km s^{-1}. The H I line was detected in 727 galaxies, with 483 of them considered good enough to be included into the 2MTF catalogue.

The Parkes radio telescope was used to observe the targets in the declination range $\delta \leq -40°$ (Hong et al. 2013). We observed 305 galaxies which did not already have high-quality H I measurements in the literature and obtained 152 well-detected H I widths (SNR > 5). Beam-switching mode with seven high-efficiency central beams was used in the Parkes observations. The multi-beam correlator produced raw spectra with a velocity resolution $\Delta v \sim 1.6$ km s^{-1}, while we measured H I widths and other parameters on the Hanning-smoothed spectra with a velocity resolution of $\sim$3.3 km s^{-1}.

All newly observed spectra from the GBT and Parkes telescope were measured by the same IDL routine *awv_fit.pro*, which based on the algorithm used by Springob et al. (2005). H I line widths were measured by five different methods (see Hong et al. 2013, section 2.1.2). We chose W_{F50} as our preferred width algorithm. This fitting method can provide accurate width measurements for low-SNR spectra. It was adopted as the preferred method by the Cornell H I digital archive and the ALFALFA blind H I survey.

2.2.3 ALFALFA data

The GBT observations did not cover the entirety of the sky north of $\delta = -40°$. 7000 deg^2 of the northern (high Galactic latitude) sky were observed by the ALFALFA survey. In this region of the sky, we rely on the ALFALFA observations, rather than making our own GBT observations. In this region, ALFALFA is expected to detect more than 30 000 H I sources with H I mass between 10^6 and $10^{10.8}$ M$_\odot$ out to $z \sim 0.06$. The ALFALFA data set has not been fully released yet. Haynes et al. (2011) published the α.40 catalogue which covers about 40 per cent of the final ALFALFA sky. However, the ALFALFA team has provided us with an updated catalogue of H I widths, current as of 2013 October. The new catalogue covers about 66 per cent of the ALFALFA sky. From this data base, the 2MTF catalogue obtained 576 H I widths. When the final ALFALFA catalogue is released, we will correspondingly update the 2MTF catalogue, making use of the complete data set.

2.3 Data collecting limit of TF sample

The initial 2MTF catalogue includes 2708 galaxies. An additional cutoff was employed to improve the data quality. Only the well-measured galaxies were included in the 2MTF peculiar velocity sample. That is, we include those galaxies with $cz \geq 600$ km s^{-1}, relative H I width error $\epsilon_w/w_{HI} \leq 10$ per cent and H I spectrum SNR ≥ 5. 141 galaxies in the template sample of Masters et al. (2008) were excluded. The current 2MTF peculiar velocity sample
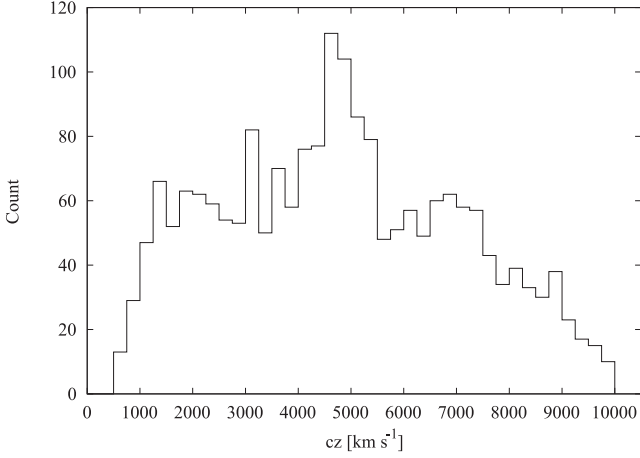
Figure 3. The redshift distribution of the 2MTF sample in the CMB frame.

has 2018 galaxies with good enough data quality for the TF distance calculations and further cosmological analysis. The sky coverage and redshift distribution of the 2MTF peculiar velocity sample are plotted in Figs 1 and 3, respectively.

3 DERIVATION OF TF DISTANCES AND PECULIAR VELOCITIES

3.1 Template relation

Using 888 spiral galaxies in 31 nearby clusters, Masters et al. (2008) built TF template relations in the 2MASS *J, H,* and *K* bands, following the approach taken by Masters et al. (2006) for SFI++, which in turn follows the approach of Giovanelli et al. (1997) for SCI. The authors found a dependence of the TF relation on galaxy morphology, with later spirals presenting a steeper slope and a dimmer zero-point on the relation than earlier type spirals. This morphological dependence occurs in all three 2MASS wavebands. The final template relations were corrected to the Sc type in the three bands, as was done for in the *I*-band relation examined by Masters et al. (2006).

We use the revised version of the Masters et al. (2008) TF relation as our template to calculate the distances of the 2MTF galaxies:

$$M_K - 5\log h = -22.188 - 10.74(\log W - 2.5),$$

$$M_H - 5\log h = -21.951 - 10.65(\log W - 2.5),$$

$$M_J - 5\log h = -21.370 - 10.61(\log W - 2.5), \qquad (1)$$

where *W* is the corrected H I width in units of km s^{-1}, and M_K, M_H, and M_J are the absolute magnitudes in the three bands separately.

3.2 TF distance and peculiar velocity calculations

Since the components of the peculiar velocity uncertainties are lognormal, our bulk flow analysis is done in logarithmic space. The main parameters used in the fitting processes are $\log(d_{\rm TF})$ and its corresponding logarithmic error. More precisely, rather than express the peculiar velocity in linear units, we work with the closely related logarithmic quantity $\log(d_z/d_{\rm TF})$, which is the logarithm of the ratio between the galaxy's redshift distance in the cosmic microwave background (CMB) frame and its TF-derived true distance. At this stage, we express this as $\log(d_z/d_{\rm TF})$, which represents the

logarithmic distance ratio before the Malmquist bias correction has been applied (see Section 3.4.) We can then express this as

$$\log\left(\frac{d_z}{d_{\rm TF}^*}\right) = \frac{-\Delta M}{5}, \qquad (2)$$

where $\Delta M = M_{\rm obs} - M(W)$ is the difference between the corrected absolute magnitude $M_{\rm obs}$ (calculated using the redshift distance of the galaxy) and the magnitude generated from the TF template relation $M(W)$ (for more details on corrected absolute magnitudes, see equation 7 from Masters et al. 2008).

The errors on the logarithmic distance ratio are the sum in quadrature of the H I width error, NIR magnitude error, inclination error, and the intrinsic error of the TF relation. Instead of using the intrinsic error estimates reported by Masters et al. (2008), we adopted new intrinsic error terms:

$$\epsilon_{{\rm int},K} = 0.44 - 0.66(\log W - 2.5),$$

$$\epsilon_{{\rm int},H} = 0.45 - 0.95(\log W - 2.5),$$

$$\epsilon_{{\rm int},J} = 0.46 - 0.77(\log W - 2.5). \qquad (3)$$

These relations were derived in magnitude units. To transform the errors into the logarithmic units used for $\log(d_z/d_{\rm TF}^*)$, one must divide the $\epsilon_{\rm int}$ values by 5. We describe the details of the new intrinsic error term estimation in Appendix A.

As shown in Fig. 2, the difference between the two sources of inclination introduces a mean scatter of 0.096, so we adopted a uniform scatter $\sigma_{\rm inc} = 0.1$ as the inclination error. The inclination uncertainty then introduces errors into the TF distances. For a galaxy with inclination b/a, we calculated the corrected H I width with $b/a \pm 0.1$, and got the corrected widths $W_{\rm high}$ and $W_{\rm low}$, respectively. Half of the difference between the two widths, $\Delta_{\rm wid,\,inc} = 0.5(W_{\rm high} - W_{\rm low})$, was then adopted as the error introduced by the inclination into the H I corrected width. Finally, the error introduced to the TF distances by inclination uncertainty, $\epsilon_{\rm inc}$, was calculated using the same approach undertaken to calculate the contribution from the HI width uncertainty, $\epsilon_{\rm wid}$.

The TF relations in the three bands are shown in Fig. 4, along with the template relations. We also show the observational errors for both the H I width and NIR magnitudes.

3.3 Member galaxies of galaxy groups

We cross-matched the 2MTF galaxies with the group list identified by Crook et al. (2007). 55 galaxy groups have more than one member in the 2MTF sample. We assume all member galaxies in a given group have the same redshift. That is, when doing the calculation in equation (2), all member galaxies in a group are assigned the group redshift $cz_{\rm group}$, while the magnitude offset ΔM was still calculated separately for each galaxy.

3.4 Malmquist bias correction

The term 'Malmquist bias' describes a set of biases originating from the spatial distribution of objects. There are two types of biases that one may consider. Inhomogeneous Malmquist bias arises from local density variations along the line of sight, and is much more pronounced when one is working in real space. This is because, as explained by Strauss & Willick (1995), the large distance errors cause the observer to measure galaxy distances scattered away from overdense regions in real space. In contrast, the much smaller redshift errors mean that this effect is insignificant in redshift space.
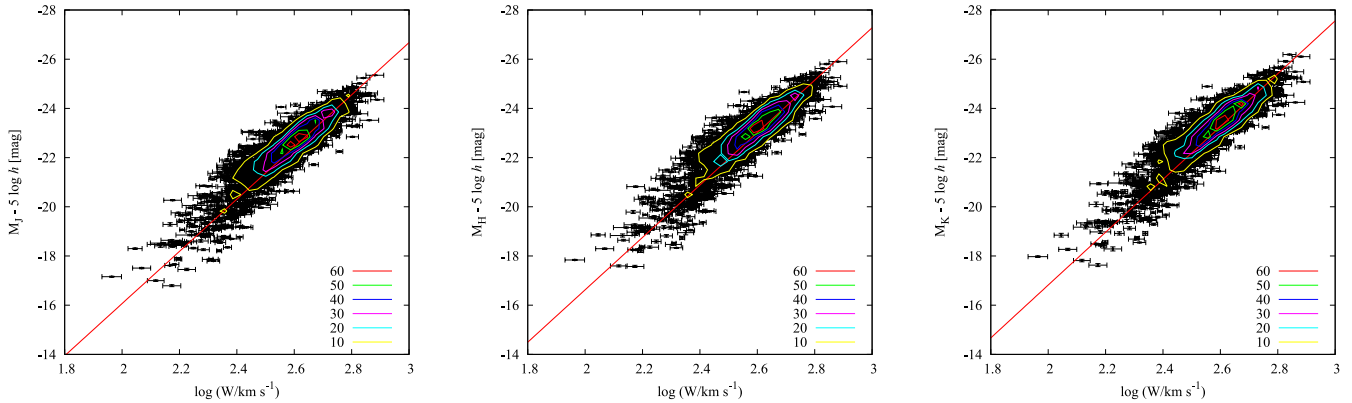
Figure 4. TF relations for 2MTF galaxies in the *J*, *H*, and *K* bands (left to right). The red solid lines are the TF template relations in the three bands. By making a 50 × 50 grid on the TF relation surface log *W*–*M*, we counted the number of galaxies falling in every grid point, and took these counts as the number density of the TF plot, which are indicated by the colour contours.

While some other TF catalogues, such as SFI++, included galaxy distances in real space, the fact that we operate in redshift space means that inhomogeneous Malmquist bias is negligible. However, we must account for the second type of Malmquist bias, homogeneous Malmquist bias.

Homogeneous Malmquist bias comes about as a consequence of the selection effects of the survey, which cause galaxies to be preferentially included or excluded from the survey, depending on their distance. Ideally, the survey selection function is a known analytical function, allowing for a relatively straightforward correction for selection effects. However, galaxy peculiar velocity surveys often have complex selection functions, requiring ad hoc approximations in the application of Malmquist bias corrections (e.g. Springob et al. 2007).

In the case of 2MTF, we used homogeneous criteria in determining which galaxies to observe. As explained in Section 2, all 2MRS galaxies with $K < 11.25$ mag, $cz < 10\,000$ km s^{-1}, and $b/a < 0.5$ that also met our morphological selection criteria were targeted for inclusion in the sample. However, many of the targeted galaxies were not included in the final sample, because there was no H I detection, the detection was marginal, or there was some other problem with the spectrum that prevented us from making an accurate TF distance estimate.

We thus adopt the following procedure for correcting for Malmquist bias (explained in more detail by Springob et al., in preparation).

(1) Using the stepwise maximum likelihood method (Efstathiou, Ellis & Peterson 1988), we derive the *K*-band luminosity function for all galaxies in 2MRS that meet our *K*-band apparent magnitude, Galactic latitude, morphological, and axis ratio criteria. For this purpose, we include galaxies beyond the 10 000 km s^{-1} redshift limit, to simplify the implementation of the luminosity function derivation. For this sample, which we designate the 'target sample', we fit a Schechter function (Press & Schechter 1974), and find $M_k^* = -23.1$ and $\alpha = -1.10$. (The stepwise maximum likelihood method does not determine the normalization of the luminosity function, but that is irrelevant for our purposes anyway.) We note that this luminosity function has a steeper faint end slope than the 2MASS *K*-band luminosity function derived by Kochanek et al. (2001), who find $\alpha = -0.87$.

(2) We next assume that the 'completeness', which in this case we take to mean the fraction of the target sample that is included in our 2MTF peculiar velocity catalogue for a given apparent

magnitude bin, is a simple function of apparent magnitude, which is the same across the sky in a given declination range. We compute this function, simply taking the ratio of observed galaxies to galaxies in the target sample for *K*-band apparent magnitude bins of width 0.25 mag, separately for two sections of the sky: north and south of $\delta = -40°$. This divide in the completeness north and south of $\delta = -40°$ is due to the fact that the GBT's sky coverage only goes as far south as $-40°$, and the galaxies south of that declination were only observed by the somewhat smaller (and therefore less sensitive) Parkes telescope.

(3) Finally, for every galaxy in the 2MTF peculiar velocity sample, we take the uncorrected $\log(d_z/d_{\text{TF}}^*)$ value, and the error ϵ_d, and compute the initial probability distribution of $\log(d_z/d_{\text{TF}})$ values, assuming that the errors follow a normal distribution in these logarithmic units. For each possible value of the logarithmic distance ratio $\log(d_z/d_{\text{TF}, i}^*)$ within 2σ of the measured $\log(d_z/d_{\text{TF}}^*)$, we weight the probability by w_i, where $1/w_i$ is the completeness (as defined in Step 2) integrated across the entire *K*-band luminosity function (derived in Step 1), evaluated at the $\log(d_z/d_{\text{TF}, i})$ in question. Note that this involves converting the completeness from a function of apparent magnitude to a function of absolute magnitude, using the appropriate distance modulus for the distance in question.

From these newly re-weighted probabilities, we calculate the mean probability-weighted log(distance), as well as the corrected logarithmic distance ratio error. This is our Malmquist bias-corrected logarithmic distance.

The histograms of the logarithmic distance ratios $\log \frac{d_{cz}}{d_{\text{TF}}}$ with the errors are shown in Figs 5 and 6, respectively. The TF distances plotted here are all Malmquist bias-corrected. A histogram of the relative errors of linear TF distances d_{TF} is plotted in Fig. 7. The mean errors of the TF distances are around 22 per cent in all three bands.

4 BULK FLOW FITTING AND THE RESULTS

4.1 χ^2 minimization method

We use χ^2 minimization to fit the peculiar velocity field to a simple bulk flow model. As mentioned in Section 3.2, the errors on peculiar velocities are lognormally distributed, so we did the fitting in logarithmic distance space, similar χ^2 logarithmic methods were adopted by Aaronson et al. (1982) and Staveley-Smith & Davies
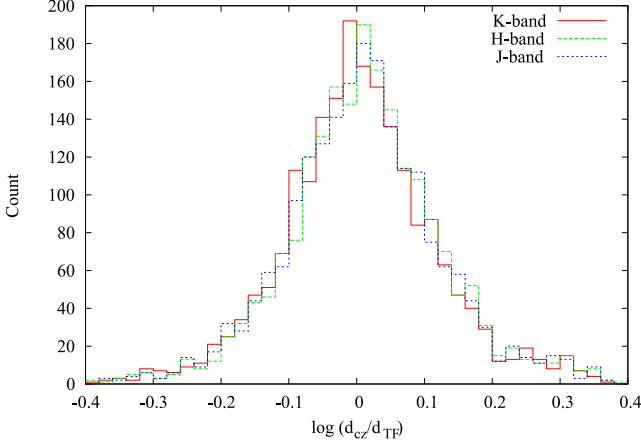
Figure 5. The histogram of logarithmic distance ratios $\log \frac{d_{cz}}{d_{TF}}$. The *K*-band data is shown by the red solid line, *H*-band data by the green dashed line, and the *J*-band data by the blue dotted line.
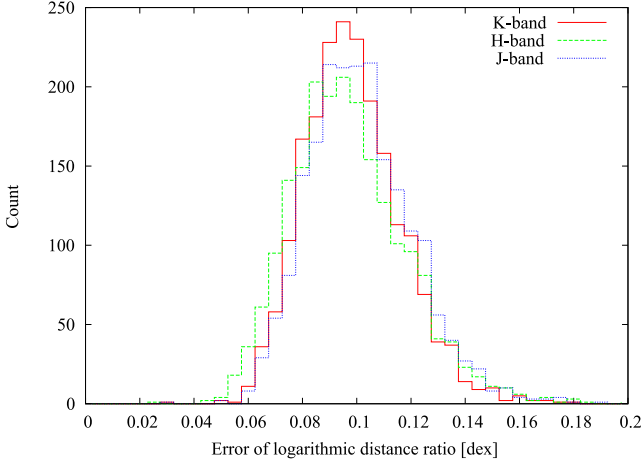
Figure 6. The histogram of the error of the logarithmic distance ratios, using the same colour scheme as in Fig. 5.
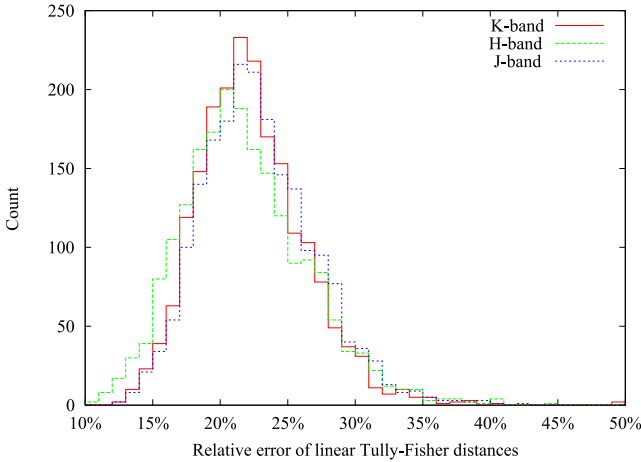
Figure 7. The histogram of the relative errors of linear TF distances, using the same colour scheme as in Fig. 5.

(1989). In the CMB frame, for a bulk flow velocity $\boldsymbol{V}$, this flow provides a radial component for each galaxy according to

$$v_{\mathrm{model},i} = \boldsymbol{V} \cdot \widehat{r}_i, \tag{4}$$

where $\widehat{r}_i$ is the unit vector pointing to the galaxy. We can also express the model-predicted distance to galaxy i as

$$d_{\mathrm{model},i} = \left(\frac{cz_i - v_{\mathrm{model},i}}{100} \right) h^{-1} \mathrm{Mpc}. \tag{5}$$

In our calculation of χ^2, we apply weights which combine the measurement errors of the logarithmic distance ratios and the weights generated from both the redshift distribution and the uneven galaxy number density in different sky areas. Our χ^2 value is given by

$$\chi^2 = \sum_{i=1}^{N} \frac{\left[\log(d_{z,i}/d_{\mathrm{model},i}) - \log(d_{z,i}/d_{\mathrm{TF},i}) \right]^2 \cdot w_i^r w_i^d}{\sigma_i^2 \cdot \sum_{i=1}^{N} (w_i^r w_i^d)}, \tag{6}$$

where σ_i is the logarithmic distance ratio error of the ith galaxy, w_i^r is the weight arising from the radial distribution of the sample, and w_i^d is the weight weighting for the uneven galaxy number density in the northern and southern sky.

The weight w_i^r was designed to make the weighted redshift distribution of the whole sample match the redshift distribution of an ideal survey. We adopted the Gaussian density profile following Watkins et al. (2009):

$$\rho(r) \propto \exp\left(-r^2/2R_I^2 \right), \tag{7}$$

with the number distribution

$$n(r) \propto r^2 \exp\left(-r^2/2R_I^2 \right), \tag{8}$$

where R_I indicates the depth of the bulk flow measurement. In this work, we adopt $R_I = 20$, 30, and 40 h^{-1} Mpc, in order to show the bulk flow across a range of depths.

Since the 2MTF sample has a denser galaxy distribution in the sky north of $\delta = -40°$, we introduced the weight w_i^d to correct the uneven number density in these two sky areas. The regions of the sky north and south of this line contain 1827 and 191 2MTF galaxies and subtend 33 885 and 7368 deg^2, respectively. This yields a ratio of galaxy number density between the southern and northern regions of roughly 1:2.08. We therefore set $w_i^d = 2.08$ for the southern objects and $w_i^d = 1$ for the northern ones.

To reduce the effect of outliers, we applied two cuts during the fitting process. With each successive cut, we did the χ^2 minimization first, and compared the difference between the bulk flow-corrected logarithmic distance ratio and the predicted Hubble flow logarithmic distance ratio: $\Delta_i = \log(d_{z,i}/d_{\mathrm{model},i}) - \log(d_{z,i}/d_{\mathrm{TF},i})$. The outliers with $\Delta_i > 3\sigma_i$ were then removed. We did the clipping twice, then applied the third χ^2 minimization, and report the result as the final bulk flow velocity. The total number of galaxies removed from the sample is around 60.

The fitting errors were calculated via the jackknife method. We built 50 jackknife subsamples by randomly removing 2 per cent of the 2MTF sample, ensuring that each galaxy was removed in one subsample only. For every jackknife subsample, the χ^2 minimization fitting was adopted, and the error on the bulk flow was taken as

$$\epsilon_V = \left[\frac{N-1}{N} \sum_{i=1}^{N} \left(V_i^J - \overline{V}^J \right)^2 \right]^{1/2}, \tag{9}$$
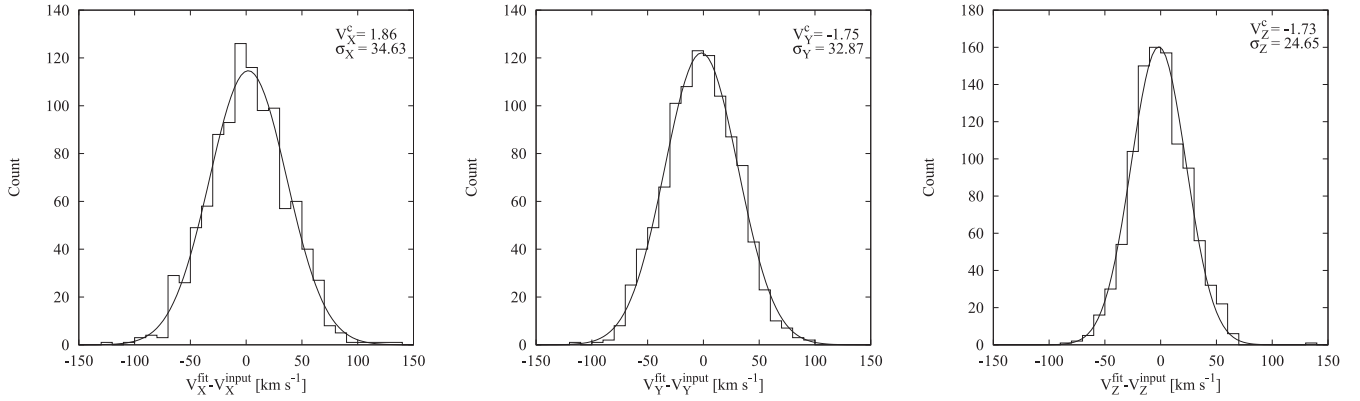
Figure 8. Histograms of the differences between the input and output bulk flow components V_X, V_Y, and V_Z for our 1000 mock samples. The solid lines show the best-fitting Gaussians to the distributions. The Gaussian centres are located at $V_X^c = 1.86$, $V_Y^c = -1.75$, and $V_Z^c = -1.73$ km s^{-1} with standard deviations of $\sigma_X = 34.63$, $\sigma_Y = 32.87$, and $\sigma_Z = 24.65$ km s^{-1}, respectively.

where $N = 50$ is the number of jackknife subsamples, V_i^J is the bulk flow for the ith jackknife subsample, and $\overline{V}^J = \frac{1}{N}\sum_{i=1}^N V_i^J$. The velocity components in three directions (V_X, V_Y, V_Z) were estimated using equation (9).

To analyse the performance of the χ^2 minimization method, we simulated 1000 mock catalogues and tested the method with these simulated data. We built the mock catalogues based on the real 2MTF data sample, with each catalogue containing 2018 mock galaxies. These galaxies have the same sky position and redshift as the real 2MTF galaxies. In each mock catalogue, we set the input bulk flow velocity equals to the same value as our measurement of the K-band data sample at the depth of $R_I = 30$ h^{-1} Mpc, i.e. $V_X = 163.4$ km s^{-1}, $V_Y = -308.3$ km s^{-1}, and $V_Z = 107.7$ km s^{-1}. We simulated distance errors by using a Gaussian random variable to induce mock scatter in the TF, with a variance equals to the total logarithmic distance error for that galaxy. The average value of this logarithmic distance error is 0.096, as in the real data.

We fit the bulk flow for each of the 1000 mock catalogues using the χ^2 minimization method, and plot the histograms of differences between the input and output bulk flow components V_X, V_Y, and V_Z in Fig. 8. We then fit the histograms using Gaussian functions, and

found the distribution of 1000 'observed' bulk flow components centred around the input values with a scatter of $\sigma_X \sim 35$ km s^{-1}, $\sigma_Y \sim 33$ km s^{-1}, and $\sigma_Z \sim 25$ km s^{-1}, respectively. The distributions present very small shifts of ~ 2 km s^{-1} in three components. This is smaller than our quoted bulk flow error by roughly an order of magnitude, and shows that the χ^2 minimization method provides an unbiased fit of the bulk flow motion.

The best-fitting χ^2 bulk flow results are presented in Table 1, subdivided by wavelength and measuring depth R_I. In all three bands with three different depths, we detected a non-zero bulk flow with a confidence level of at least 3σ.

In addition to the bulk flow measurements for individual wavebands, we have also combined the data from all three wavebands into a composite measurement of the bulk flow. That is, each galaxy appears in this sample three times, but with different peculiar velocities as measured in each of the wavebands. But we have applied the χ^2 minimization method so that each of the three peculiar velocity measurements for a given galaxy is counted separately in equation (6). We then compute the error using the same jackknife method. Though once a galaxy was removed from a subsample, all three peculiar velocities belonging to this galaxy were removed together. We report

Table 1. Best-fitting χ^2 measured bulk flow of the 2MTF sample in J, H, and K bands. The velocity components (V_X, V_Y, V_Z) are calculated in Galactic Cartesian coordinates.

	Amplitude (km s^{-1})	l (deg)	b (deg)	V_X (km s^{-1})	V_Y (km s^{-1})	V_Z (km s^{-1})	χ^2/d.o.f.
J band							
$R_I = 20$ h^{-1} Mpc	303.5 ± 22.2	306.7 ± 7.3	11.9 ± 4.9	177.4 ± 29.2	-238.2 ± 17.0	62.5 ± 22.2	0.98
$R_I = 30$ h^{-1} Mpc	319.0 ± 28.0	297.5 ± 4.1	18.5 ± 4.6	139.6 ± 17.5	-268.4 ± 27.9	101.1 ± 26.9	0.95
$R_I = 40$ h^{-1} Mpc	319.4 ± 21.3	290.8 ± 4.2	11.4 ± 4.7	111.3 ± 20.9	-292.7 ± 19.8	63.0 ± 25.6	0.95
H band							
$R_I = 20$ h^{-1} Mpc	345.7 ± 53.6	308.7 ± 7.8	18.1 ± 13.9	205.7 ± 54.4	-256.3 ± 43.5	107.1 ± 82.2	1.07
$R_I = 30$ h^{-1} Mpc	352.4 ± 34.4	296.9 ± 5.6	26.8 ± 11.6	142.4 ± 29.6	-280.6 ± 31.7	158.7 ± 65.2	1.04
$R_I = 40$ h^{-1} Mpc	319.1 ± 37.4	296.2 ± 8.3	5.1 ± 6.1	140.5 ± 51.1	-285.0 ± 28.2	28.4 ± 33.6	1.00
K band							
$R_I = 20$ h^{-1} Mpc	301.3 ± 27.3	305.4 ± 8.2	8.5 ± 6.4	172.6 ± 42.1	-243.0 ± 30.5	44.4 ± 39.6	1.00
$R_I = 30$ h^{-1} Mpc	365.1 ± 36.2	297.9 ± 6.1	17.2 ± 5.5	163.4 ± 36.8	-308.3 ± 44.5	107.7 ± 33.8	0.98
$R_I = 40$ h^{-1} Mpc	331.1 ± 22.5	292.0 ± 3.4	11.8 ± 4.2	121.4 ± 25.0	-300.5 ± 19.6	67.9 ± 20.8	0.96
3 bands combined							
$R_I = 20$ h^{-1} Mpc	310.9 ± 33.9	287.9 ± 5.9	11.1 ± 3.4	93.7 ± 34.4	-290.4 ± 28.9	59.8 ± 18.4	0.90
$R_I = 30$ h^{-1} Mpc	280.8 ± 25.0	296.4 ± 16.1	19.3 ± 6.3	117.8 ± 68.3	-237.4 ± 30.6	92.9 ± 29.4	0.93
$R_I = 40$ h^{-1} Mpc	292.3 ± 27.8	296.5 ± 9.8	6.5 ± 9.2	129.6 ± 47.6	-259.9 ± 37.6	33.0 ± 46.6	0.95

these composite measurements of the bulk flow as '3 bands combined' in Table 1.

4.2 Additional bulk flow fitting methods

In addition to the χ^2 minimization method used in Section 4.1, we have done additional fits of the bulk flow using the maximum likelihood estimator (MLE; Kaiser 1988) and the MV method (Watkins et al. 2009; Feldman et al. 2010). Both methods involve converting the logarithmic distance ratios into linear peculiar velocities, and then applying the appropriate weights, which depend on sky position. We thus have

$$V = \sum_{n=1}^{N} w_n v_n, \tag{10}$$

where v_n is the linear peculiar velocity of galaxy n, and w_n is the corresponding weight applied to the galaxy such that one recovers the bulk flow V. The optimal approach for converting the logarithmic distance ratios into linear peculiar velocities for use in these methods is explained in detail by Scrimgeour et al. (submitted), who apply these methods to the 6dF Galaxy Survey peculiar velocities (Springob et al., submitted). The advantage of these methods over the χ^2 approach described in Section 4.1 is that the weighting accounts for the sample selection on the sky, with more densely sampled regions being weighted differently from less densely sampled regions. The advantage of the χ^2 minimization approach, however, is that the fitting is done in the logarithmic distance units in which the errors are roughly Gaussian.

4.2.1 Maximum likelihood method

Following Kaiser (1988), the MLE bulk flow weights are

$$w_{i,n} = \sum_j A_{i,j}^{-1} \frac{\widehat{r}_{n,j}}{\sigma_n^2 + \sigma_*^2}, \tag{11}$$

where

$$A_{i,j} = \sum_n \frac{\widehat{r}_{n,i}\widehat{r}_{n,j}}{\sigma_n^2 + \sigma_*^2}, \tag{12}$$

where σ_n is the uncertainty on the velocity v_n which is calculated following Scrimgeour et al. (submitted), and σ_* is the 1D velocity dispersion.

4.2.2 Minimum variance method

The MV weighting scheme, as proposed by Watkins et al. (2009) and Feldman et al. (2010), gives us an N-dimensional vector of weights specifying the ith moment u_i, which are given by

$$\boldsymbol{w}_i = (\mathbf{G} + \lambda \boldsymbol{P})^{-1} \boldsymbol{Q}_i \tag{13}$$

where $\boldsymbol{w}_i$ is the vector of weights for each galaxy in the ith direction. $\mathbf{G}$ is the covariance matrix of the individual velocities, which includes both a noise term and a cosmic variance term determined by an input model power spectrum. $\boldsymbol{P}$ is the $k = 0$ limit of the angle-averaged window function of the galaxies, and $\boldsymbol{Q}_i$ incorporates the input ideal window function. The λ term is a Lagrange multiplier. The MV method weights the bulk flow measurements to a given ideal survey, which we have chosen to be the same Gaussian profile with the χ^2 minimization method (equations 7 and 8) with $R_I = 20$, 30, and 40 h^{-1} Mpc. See Watkins et al. (2009) and Feldman et al. (2010) for more details on the method.

The resulting MLE and MV measurements of the bulk flow are presented in Table 2, and they largely agree with the χ^2 minimization method. We discuss these results further in the following section.

5 DISCUSSION

In Table 1, we list 12 χ^2 minimization measured bulk flow velocities from the three 2MASS NIR wavebands and the '3 bands combined' sample, each using three sample depths. To simplify the discussion here, we focus on our best measurements of the bulk flow at the three depths, which are the measurements taken from the combined sample.

Using the combined data with a depth $R = 30$ h^{-1} Mpc, we detected a bulk flow velocity in the direction of $l = 296°.4 \pm 16°.1$, $b = 19°.3 \pm 6°.3$. Our direction is consistent with that of most previous studies, but our result tends to have a higher galactic latitude.

Table 2. MV and MLE bulk flow of the 2MTF sample in J, H, and K bands. The errors quoted are noise-only, with noise+cosmic variance in parentheses.

	Amplitude (km s^{-1})	l (deg)	b (deg)	V_X (km s^{-1})	V_Y (km s^{-1})	V_Z (km s^{-1})
J band						
MV ($R_I = 20$ h^{-1} Mpc)	$313 \pm 33(150)$	295 ± 7	13 ± 6	$129 \pm 35(174)$	$-276 \pm 33(173)$	$71 \pm 30(172)$
MV ($R_I = 30$ h^{-1} Mpc)	$328 \pm 39(137)$	283 ± 7	12 ± 6	$72 \pm 39(151)$	$-313 \pm 39(153)$	$68 \pm 36(150)$
MV ($R_I = 40$ h^{-1} Mpc)	$325 \pm 49(132)$	275 ± 9	7 ± 8	$27 \pm 48(144)$	$-321 \pm 50(147)$	$41 \pm 45(142)$
MLE	351 ± 28	295 ± 5	17 ± 4	143 ± 30	-304 ± 28	100 ± 21
H band						
MV ($R_I = 20$ h^{-1} Mpc)	$294 \pm 33(149)$	294 ± 7	13 ± 6	$177 \pm 35(173)$	$-261 \pm 33(172)$	$67 \pm 30(173)$
MV ($R_I = 30$ h^{-1} Mpc)	$317 \pm 39(135)$	283 ± 7	14 ± 7	$70 \pm 39(151)$	$-300 \pm 39(153)$	$75 \pm 36(150)$
MV ($R_I = 40$ h^{-1} Mpc)	$308 \pm 48(132)$	275 ± 9	10 ± 8	$29 \pm 48(144)$	$-302 \pm 49(147)$	$55 \pm 45(142)$
MLE	338 ± 28	294 ± 5	18 ± 4	133 ± 30	-292 ± 28	104 ± 21
K band						
MV ($R_I = 20$ h^{-1} Mpc)	$305 \pm 33(149)$	292 ± 7	13 ± 6	$109 \pm 34(172)$	$-276 \pm 33(174)$	$71 \pm 29(173)$
MV ($R_I = 30$ h^{-1} Mpc)	$313 \pm 39(134)$	276 ± 7	13 ± 7	$33 \pm 39(151)$	$-303 \pm 40(153)$	$70 \pm 36(149)$
MV ($R_I = 40$ h^{-1} Mpc)	$312 \pm 49(132)$	270 ± 9	11 ± 8	$1 \pm 48(145)$	$-306 \pm 50(147)$	$59 \pm 45(142)$
MLE	345 ± 27	295 ± 5	16 ± 4	141 ± 30	-300 ± 28	95 ± 21

Table 3. Bulk flow directions from previous studies.

	l (deg)	b (deg)	Reference
2MTF	**296.4 ± 16.1**	**19.3 ± 6.3**	**This work**
COMPOSITE	287 ± 9	8 ± 6	Watkins et al. (2009)
FWH10	282 ± 11	6 ± 6	Feldman et al. (2010)
ND11	276 ± 3	14 ± 3	Nusser & Davis (2011)
DKS11	290^{+39}_{-31}	20^{+32}_{-32}	Dai et al. (2011)
A1	319 ± 25	7 ± 13	Turnbull et al. (2012)
MP14	281 ± 7	8^{+6}_{-5}	Ma & Pan (2014)

We list our χ^2 minimization measured bulk flow directions, along with the results from previous studies in Table 3. An Aitoff projection of bulk flow directions is also presented in Fig. 9.

The expected amplitude of the bulk flow is strongly dependent on the characteristic depth of the galaxies being sampled (Li et al. 2012; Ma & Pan 2014). As survey geometry and source selection criteria vary greatly between surveys, one must account for this in comparing the bulk flow amplitude to cosmological expectations.

In the ΛCDM model, the variance of the bulk flow velocity in a spherical region R is

$$v_{\rm rms}^2 = \frac{H_0^2 f^2}{2\pi^2} \int W^2(kR)P(k)\mathrm{d}k, \tag{14}$$

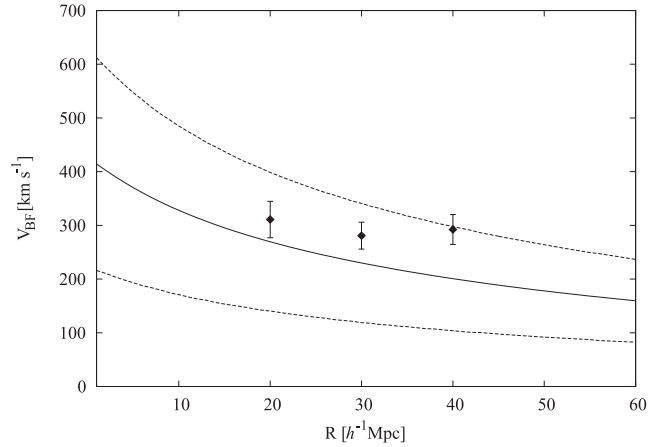where k is the wavenumber, $W(kR) = \exp(-k^2R^2)/2$ is the Fourier transform of a Gaussian window function, $P(k)$ is the matter power spectrum (we used the matter power spectrum generated by the CAMB package; Lewis, Challinor & Lasenby 2000), $f = \Omega_{\rm m}^{0.55}$ is the linear growth rate, and H_0 is the Hubble constant.

The probability distribution function of the bulk flow V is (Li et al. 2012)

$$p(V)\mathrm{d}V = \sqrt{\frac{2}{\pi}} \left(\frac{3}{v_{\rm rms}^2}\right)^{3/2} V^2 \exp\left(-\frac{3V^2}{2v_{\rm rms}^2}\right) \mathrm{d}V. \tag{15}$$

Figure 10. The comparison between the bulk flow velocity amplitude from the 2MTF sample and the ΛCDM prediction using the *WMAP*-7 yr parameters (Larson et al. 2011). The diamonds with error bars indicate the bulk flow velocity amplitude measured from the 2MTF '3 bands combined' sample using the χ^2 minimization method, with the depth $R_I = 20$, 30, and 40 h^{-1} Mpc, respectively. The solid line shows the theoretical curve and the dashed lines indicate the sample variance at the 1σ level.

The PDF here is normalized. By setting $\mathrm{d}p(V)/\mathrm{d}V = 0$, the peak of the distribution can be easily calculated: $v_{\rm peak} = \sqrt{2/3}v_{\rm rms}$. We adopt this peak velocity as the bulk velocity amplitude predicted by the ΛCDM model.

We show the 3 bands combined measurement of χ^2 minimization method in Fig. 10 together with the model predicted curve. The 1σ variance of the bulk flow velocity is also plotted as a dashed line. Our results agree with the model predicted bulk flow amplitude at the 1σ level. Thus, our results support the conclusions reported by some previous studies (e.g. Dai et al. 2011; Nusser & Davis 2011; Turnbull et al. 2012; Kitaura et al. 2012; Rathaus et al. 2013; Ma & Pan 2014) that the bulk flow detected in the local Universe is consistent with the ΛCDM model.
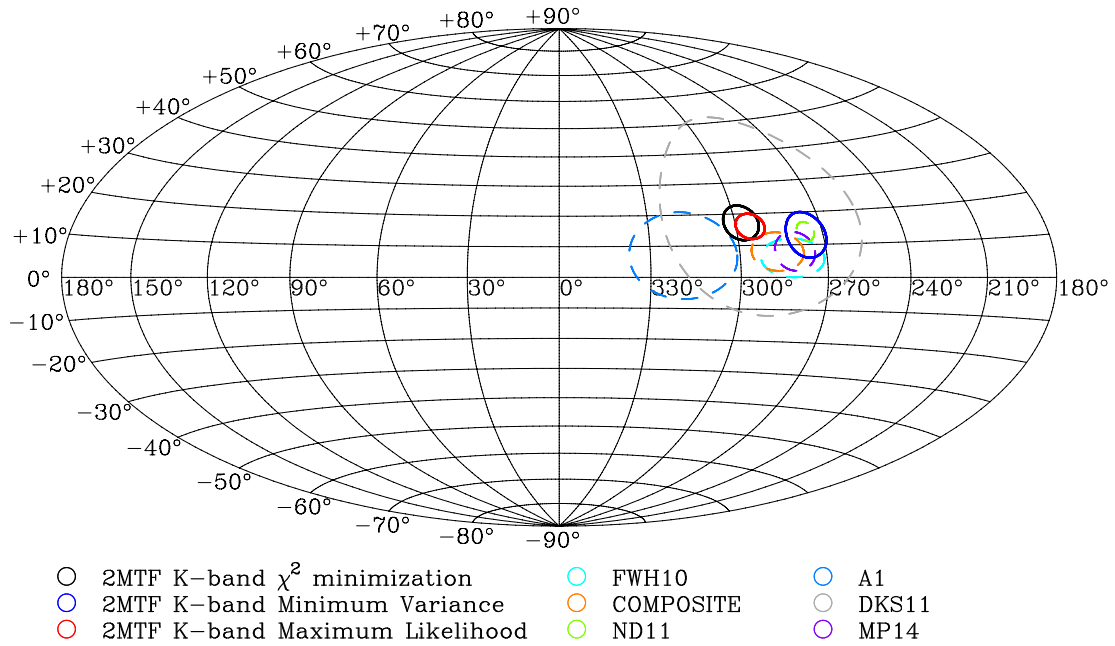

Figure 9. The direction of the measured bulk flow velocities, using an Aitoff projection and Galactic coordinates. The red circle shows the bulk flow direction estimated from '3 bands combined' sample with depth $R_I = 30$ h^{-1} Mpc. The size of the circles indicates the 1σ error of the direction. The bulk flow directions from several previous studies are also plotted for comparison. The references for these literature results are listed in Table 3.

Figure 11. The direction of the measured bulk flow velocities, using an Aitoff projection and Galactic coordinates. The black, blue, and red circles show the bulk flow direction determined from the K-band sample by the χ^2 minimization ($R_I = 30\ h^{-1}$ Mpc), MV ($R_I = 30\ h^{-1}$ Mpc), and maximum likelihood methods, respectively. The size of the circles indicates the 1σ error. The literature bulk flow directions are plotted by dashed circles.
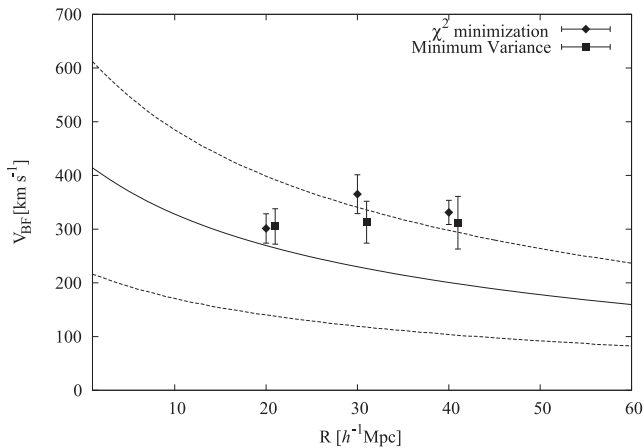
Figure 12. The comparison between the bulk flow amplitudes measured by χ^2 minimization method (diamonds) and MV method (squares) on 2MTF K-band sample. The MV method results are shifted 1 h^{-1} Mpc right to make the comparison clear. The solid line shows the theoretical curve and the dashed lines indicate the variance at the 1σ level.

As a point of comparison, both the MV and MLE results are shown in Table 2. The MV calculation is performed for the same 20, 30, and 40 h^{-1} Mpc depths used for the χ^2 minimization method, while the MLE method only samples one depth. The measurements largely agree with the χ^2 minimization results in both amplitude and direction. A comparison of bulk flow measurements on 2MTF K-band sample is shown in Figs 11 and 12.

6 CONCLUSIONS

The bulk flow motion is the dipole component of the peculiar velocity field, thought to be induced by the gravitational attraction of large-scale structures. Therefore, its measurement can help to constrain cosmological models.

The 2MTF survey is an all-sky TF survey, using photometric data from the 2MASS catalogue and H I data from existing published works and new observations. Using this data set, we have derived peculiar velocities for 2018 galaxies in the local Universe ($cz \leq 10\,000$ km s^{-1}). This sample covers all of the sky down to a Galactic latitude $|b| = 5°$, providing better sky-coverage than previous surveys.

We applied a χ^2 minimization method to the peculiar velocity catalogue to estimate the bulk flow motion. We applied three Gaussian window functions located at three different depths ($R_I = 20$, 30, and 40 h^{-1} Mpc) to the catalogues generated by three NIR bands (J, H, and K). Our tightest constraints came from combining the data in all three bands, which gave us bulk flow amplitudes of $V = 310.9 \pm 33.9$, 280.8 ± 25.0, and 292.3 ± 27.8 km s^{-1} for $R_I = 20$, 30 and 40 h^{-1} Mpc, respectively. Similar results are found when we apply the maximum likelihood and MV methods of Kaiser (1988) and Watkins et al. (2009), respectively. We find that these amplitudes all agree with the ΛCDM model prediction at the 1σ level. The directions of our estimated bulk flow are also consistent with previous probes.

REFERENCES

Aaronson M., Huchra J., Mould J., Schechter P. L., Tully R. B., 1982, ApJ, 258, 64

Crook A. C., Huchra J. P., Martimbeau N., Masters K. L., Jarrett T., Macri L. M., 2007, ApJ, 655, 790

Dai D.-C., Kinney W. H., Stojkovic D., 2011, J. Cosmol. Astropart. Phys., 4, 15

Djorgovski S., Davis M., 1987, ApJ, 313, 59

Dressler A., Lynden-Bell D., Burstein D., Davies R. L., Faber S. M., Terlevich R., Wegner G., 1987, ApJ, 313, 42

Efstathiou G., Ellis R. S., Peterson B. A., 1988, MNRAS, 232, 431

Feldman H. A., Watkins R., Hudson M. J., 2010, MNRAS, 407, 2328

Giovanelli R., Haynes M. P., Herter T., Davies R. L., Faber S. M., Terlevich R., Wegner G., 1997, AJ, 113, 53

Giovanelli R. et al., 2005, AJ, 130, 2598

Haynes M. P. et al., 2011, AJ, 142, 170

Hong T. et al., 2013, MNRAS, 432, 1178

Huchra J. P. et al., 2012, ApJS, 199, 26

Hudson M. J., Smith R. J., Lucey J. R., Branchini E., 2004, MNRAS, 352, 61

Jarrett T. H., Chester T., Cutri R., Schneider S., Skrutskie M., Huchra J. P., 2000, AJ, 119, 2498

Kaiser N., 1988, MNRAS, 231, 149

Kitaura F.-S., Erdoğdu P., Nuza S. E., Khalatyan A., Angulo R. E., Hoffman Y., Gottlöber S., 2012, MNRAS, 427, L35

Kochanek C. S. et al., 2001, ApJ, 560, 566

Larson D. et al., 2011, ApJS, 192, 16

Lewis A., Challinor A., Lasenby A., 2000, ApJ, 538, 473

Li M. et al., 2012, ApJ, 761, 151

Ma Y.-Z., Pan J., 2014, MNRAS, 437, 1996

Ma Y.-Z., Scott D., 2013, MNRAS, 428, 2017

Ma Y.-Z., Branchini E., Scott D., 2012, MNRAS, 425, 2880

Masters K. L., Springob C. M., Haynes M. P., Giovanelli R., 2006, ApJ, 653, 861

Masters K. L., Springob C. M., Huchra J. P., 2008, AJ, 135, 1738

Masters K. L., Crook A., Hong T., Jarrett T. H., Koribalski B. S., Macri L., Springob C. M., Staveley-Smith L., 2014, MNRAS, 443, 1044

Mathewson D. S., Ford V. L., Buchhorn M., 1992, ApJS, 81, 413

Nusser A., Davis M., 2011, ApJ, 736, 93

Paturel G., Theureau G., Bottinelli L., Gouguenheim L., Coudreau-Durand N., Hallet N., Petit C., 2003, A&A, 412, 57

Phillips M. M., 1993, ApJ, 413, L105

Press W. H., Schechter P., 1974, ApJ, 187, 425

Rathaus B., Kovetz E. D., Itzhaki N., 2013, MNRAS, 431, 3678

Springob C. M., Haynes M. P., Giovanelli R., Kent B. R., 2005, ApJS, 160, 149

Springob C. M., Masters K. L., Haynes M. P., Giovanelli R., Marinoni C., 2007, ApJS, 172, 599

Staveley-Smith L., Davies R. D., 1989, MNRAS, 241, 787

Strauss M. A., Willick J. A., 1995, Phys. Rep., 261, 271

Theureau G., Bottinelli L., Coudreau-Durand N., Gouguenheim L., Hallet N., Loulergue M., Paturel G., Teerikorpi P., 1998, A&AS, 130, 333

Theureau G. et al., 2005, A&A, 430, 373

Theureau G., Hanski M. O., Coudreau N., Hallet N., Martin J.-M., 2007, A&A, 465, 71

Tully R. B., Fisher J. R., 1977, A&A, 54, 661

Turnbull S. J., Hudson M. J., Feldman H. A., Hicken M., Kirshner R. P., Watkins R., 2012, MNRAS, 420, 447

Watkins R., Feldman H. A., Hudson M. J., 2009, MNRAS, 392, 743

APPENDIX A: NEW INTRINSIC ERROR ESTIMATION

As described in Section 2.1, Masters et al. (2008) estimated the intrinsic errors of the TF relation using the 888-galaxy template sample with *I*-band axis ratio. However, we have adopted the 2MASS co-added axis ratio for the 2MTF sample. Thus, we must make a new estimate of the intrinsic scatter in the TF relation, appropriate for the co-added axis ratio. We have calculated the new intrinsic errors by subtracting the observed error components from the total scatter of the distribution.

We assume that a proper error estimation should approximately match the total scatter of the data sample:

$$\sigma^2 \sim \epsilon_{\text{total}}^2 = \epsilon_{\text{wid}}^2 + \epsilon_{\text{ran}}^2 + \epsilon_{\text{mag}}^2 + \epsilon_{\text{inc}}^2 + \epsilon_{\text{int}}^2, \tag{A1}$$

where σ is the scatter of the data points related to the TF template, ϵ_{wid} is the error of the H I widths, $\epsilon_{\text{ran}} = 268$ km s^{-1} is the assumed mean rms of velocities for field galaxies (see details in Appendix B), ϵ_{mag} is the error on the 2MASS magnitudes, ϵ_{inc} is the error introduced by the 2MASS co-added inclinations, ϵ_{int} is the intrinsic error of the TF relation. All errors and scatter in equation (A1) are in logarithmic units.

The residual component or intrinsic error is

$$\epsilon_{\text{int}}^2 \sim \sigma^2 - \left(\epsilon_{\text{wid}}^2 + \epsilon_{\text{ran}}^2 + \epsilon_{\text{mag}}^2 + \epsilon_{\text{inc}}^2 \right). \tag{A2}$$

We assume a linear relation between the intrinsic error and logarithmic H I widths log W

$$\epsilon_{\text{int}} = a \log W + b, \tag{A3}$$

where a and b are free parameters.

The final results are the intrinsic error terms reported by equation (3). We show the error components along with the total scatter of the *K*-band sample in the Fig. A1. Using the new intrinsic error, the total error closely matches the total scatter.

APPENDIX B: THE RANDOM MOTION OF GALAXIES

Ideally, the intrinsic error of the TF relation would be estimated using a galaxy cluster sample. All of the galaxies in the same cluster are assumed to be at the same distance, thus subtracting out the
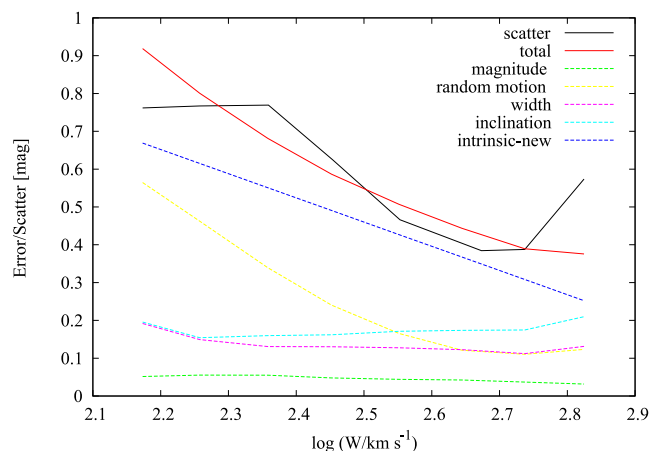
Figure A1. A plot of different error components of the *K*-band data as a function of the logarithmic H I width. The blue dashed line indicates the new intrinsic error term. The red line shows our estimate of the final total error in the data, which matches the observed scatter of the sample well.
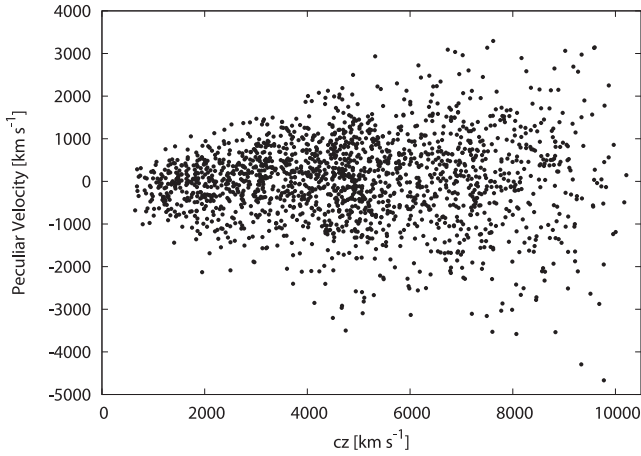
Figure B1. Peculiar velocities versus redshift for the 2018 2MTF field galaxies.
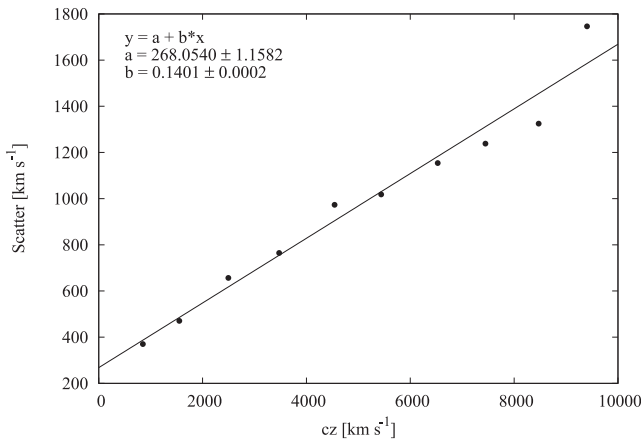
Figure B2. Mean scatter of peculiar velocity as a function of redshift, with the best-fitting linear relation superimposed.

individual motions of the galaxies themselves. However, when estimating the new intrinsic error term, we used the data of 2018 field galaxies. The uncorrected random motions of these galaxies would introduce a spurious component into the scatter of the TF relation.

To remove this effect, we need to estimate the mean random motion of galaxies in our sample. We start by calculating the peculiar velocity of the field galaxies using the TF relation template from equation (1). Instead of the logarithmic quantity $\log(d_z/d_{\rm TF})$, a linear low-redshift approximation

$$v_{\rm pec} = cz \left(1 - 10^{\frac{\Delta M}{5}}\right) \tag{B1}$$

is adopted to generate the peculiar velocities of galaxies. We then place the galaxies on to the redshift – peculiar velocity diagram Fig. B1, and calculate peculiar velocity scatter in redshift bins of width 1000 km s^{-1}. As expected, the scatter increases with redshift, owing to the fact that most of the observational errors scale with distance. To find the pure random motion velocity of the galaxies, we do a linear fit to the scatter as a function of redshift, and extended the linear relation to $cz = 0$ km s^{-1}. We adopt this zero-point as the underlying rms of our velocities. As shown in Fig. B2, we found $v_{\rm ran} = 268$ km s^{-1}, which is close to the commonly used value of $v_{\rm ran} = 300$ km s^{-1} (e.g. Strauss & Willick 1995; Masters et al. 2006).

This paper has been typeset from a TₑX/LᴬTₑX file prepared by the author.